CHIN. PHYS. LETT. Vol. 37, No. 10 (2020) 106201

Effect of B-Site Ordering on the Magnetic Order in Multifunctional La_2NiMnO_6 Double Perovskite

Dexin Yang(杨得鑫)[1*], Rui Jiang(蒋蕊)[1], Yaohua Zhang(张耀华)[1], Hui Zhang(张辉)[1], Senlin Lei(雷森林)[1], Tao Yang(杨涛)[1], Xiaoshi Hu(胡小诗)[1], Shuai Huang(黄帅)[1], Jingyuan Ge(葛景园)[2], Kunpeng Su(苏昆朋)[1], Haiou Wang(王海鸥)[1], and Dexuan Huo(霍德璇)[1*]

[1] *College of Materials & Environmental Engineering, Hangzhou Dianzi University, Hangzhou 310018, China*
[2] *College of Chemistry and Materials Engineering, Wenzhou University, Wenzhou 325035, China*

(Received 13 July 2020; accepted 25 August 2020; published online 29 September 2020)

To obtain various Ni/Mn orderings, we use a low-temperature synthesized method to modulate the Ni/Mn ordering of the ferromagnetic-ferroelastic La_2NiMnO_6 compound, and the Ni/Mn ordering is estimated by the low-temperature saturation magnetism. The microstructures, crystal structures and magnetic properties are investigated, and the Landau theory are used to describe the form and magnitude of the coupling effects between Ni/Mn ordering and magnetic order parameters. It is predicted that the Ni/Mn ordering would be a strong coupling effect with the Curie transition temperatures if the La_2NiMnO_6 sample stoichiometry is close.

PACS: 62.20.de, 62.40.+i, 64.60.−i, 75.40.−s DOI: 10.1088/0256-307X/37/10/106201

Double perovskite La_2NiMnO_6 (LNMO) is a rare example of a single-material platform with multiple functions, which is a ferromagnetic-ferroelastic semiconductor with excellent magneto-dielectric coupling property near room temperature.[1−4] Therefore, it has the potential applications in the fields of spintronics[5−9] and electric devices,[1] and as an electrocatalyst for efficient electrocatalytic oxygen evolution.[10] The complex magnetic, electric, dielectric properties and their coupling behavior have been extensively investigated. However, many conflicting experimental results are obtained for different LNMO samples. For example, we find that the Curie temperatures and low-temperature saturation temperatures from Pal *et al.*[3] and Zhao *et al.*[11] are significantly different. Their differences are mainly due to the B-site disordering (or Ni/Mn disordering).[4] Generally, the B-site disordering[1,2,12−16] have strong influences on their physical properties, which in turn have a strong correlation with the synthesized conditions.[17]

In the present work, we use the molten-salt-mediated (MSM) method to obtain LNMO samples with different Ni/Mn orderings, which is an ideal method to modulate the microstructures and particle sizes of perovskites.[18−20] For example, Fuoco *et al.*[18] successfully prepared the half-metallic double perovskites of Sr_2FeReO_6, Ba_2FeReO_6 and Sr_2CrReO_6 in high purity and homogeneity using a NaCl/KCl molten flux at 750–800℃. However, to the best of our knowledge, the flux synthesized method has not yet been reported for LNMO samples. Reported herein are the flux-mediated syntheses of LNMO samples using NaCl and NaCl/KCl salt mixtures. The influences of the salts and annealing process on the microstructures, saturation magnetization M_s, T_c, Q_{od}, etc. are studied. The samples prepared in this study are labeled as LNMO_750C_Na+K, LNMO_850C_Na, LNMO_1350C_Na, and LNMO_1350C, and the detailed synthesized processes are demonstrated in the Supplementary Material. The measurements of the x-ray diffraction (XRD), scanning electron microscopy (SEM) and magnetization are performed, and the detailed descriptions are shown in the Supplementary Material.

Finally, several LNMO samples with different Ni/Mn orderings are successfully synthesized, and it is, thus, a base for us to discuss the role of Q_{od} on the m_3 in LNMO through the space group and the Landau theory.[21] The coupling between Q_{od} and m_3 in LNMO samples are normally mediated by the lattice strains due to the long interactions which is provided by the strain fields.[22,23] In addition, Q_{od} could be described by the irreducible representation R_1^+ of holosymmetric space group $Pm\bar{3}m$.[21] Moreover, a Landau description is developed to provide a method of rationalizing and testing the strength of the coupling coefficient λ, depending on the data in this study and a compilation of data from the literature.

The Rietveld refinement analysis results of the room-temperature XRD for samples LNMO_750C_Na+K, LNMO_850C_Na, LNMO_1350C_Na and LNMO_1350C are shown in Fig. 1, and the fit parameters of the refinement result are listed in Table 1. The highly or partially

Supported by the National Natural Science Foundation of China (Grant Nos. 51702289, 21801054 and 11604067), and the Natural Science Foundation of Zhejiang Province (Grant No. LQ20E020006).
*Corresponding authors. Email: dy263@hdu.edu.cn; dxhuo@hdu.edu.cn
© 2020 Chinese Physical Society and IOP Publishing Ltd

B-site ordered LNMO double perovskite exhibits a typical rock salt structure in which ordered Ni^{2+} (d^8: $t_{2g}^6e_g^2$, $S = 2/2$) and Mn^{4+} (d^3: $t_{2g}^3e_g^0$, $S = 3/2$) ions occupy the metal (M) centers of corner-sharing MO_6 octahedra.[1,16] The refined results show that all the samples have the co-existence feature of monoclinic ($P2_1/n$, No. 14) and rhombohedral ($R\bar{3}$, No. 148) phases. This feature coincides well with the previous results in literature that $P2_1/n$ and $R\bar{3}$ structures typically coexist over a significant temperature range including the room temperature.[1,16,24] They have subtle differences that could be due to the annealing process and the influence of the salts.

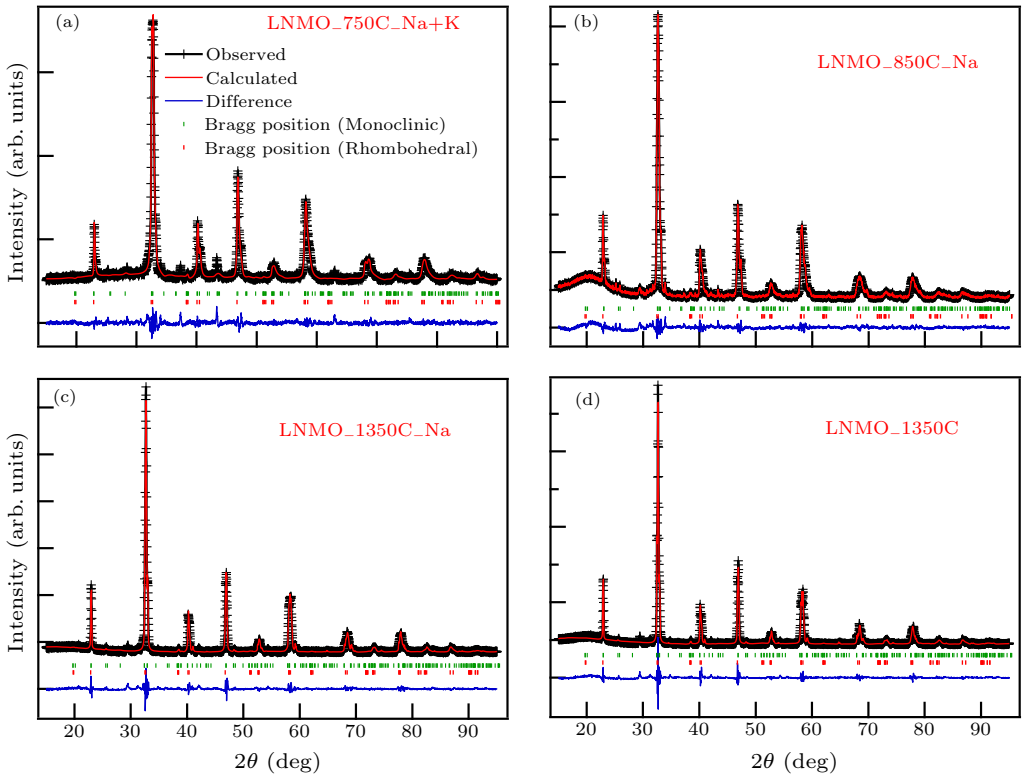

Fig. 1. Room temperature XRD Rietveld refinement result of samples (a) LNMO_750C_Na+K; (b) LNMO_850C_Na; (c) LNMO_1350C_Na; and (d) LNMO_1350C. Observed profile is indicated by the black cross shape and the calculated profile by the red solid line. Bragg peak positions are shown by the green ($P2_1/n$ phase) and red ($R\bar{3}$) vertical peaks, and the difference diffractogram (difference between the observed data and the calculated results) is shown as the blue solid line.

Table 1. Structural refinement results from powder x-ray diffraction.

Samples		LNMO_1350C	LNMO_750C_Na+K	LNMO_850C_Na	LNMO_1350C_Na
Prepared temperature		1350℃	750℃	850℃	1350℃
Flux			NaCl/KCl	NaCl	NaCl
Ratio of $P2_1/n$ to $R\bar{3}$		24.91%:75.09%	73.37%:26.63%	52.92%:47.08%	20.82%:79.18%
$P2_1/n$ phase	a (Å)	5.4455(3)	5.480(2)	5.442(2)	5.4409(3)
	b (Å)	5.5151(3)	5.505(3)	5.4789(16)	5.5179(4)
	c (Å)	7.7408(3)	7.7509(19)	7.7023(16)	7.7364(3)
	β (deg)	88.816(5)	89.45(4)	88.77(3)	88.756(5)
$R\bar{3}$ phase	a (Å)	5.4797(2)	5.4741(6)	5.4714(7)	5.4798(3)
	α (deg)	60.265(3)	60.446(5)	60.482(10)	60.237(4)
R_p (%)		9.2	6.9	7.3	8.3
R_{exp} (%)		5.0	6.8	4.9	5.3
χ^2		2.3	1.4	2.0	2.1

The SEM images in Fig. 2 show the particle sizes and morphologies of the LNMO samples, and the results imply that the selected salts and annealing temperature have important influences on the microstructures of LNMO. As shown in Fig. 2(a), well-faced octahedral particles are successfully prepared, and the sizes of the particles are in the range 500–1000 nm. According to the x-ray result, most of the particles are composed of the monoclinic crystals in sample LNMO_750C_Na+K. Correspondingly, the particles are rectangular parallelepiped with obvious corner angles, and their sizes are less than 500 nm [Fig. 2(b)] in

sample LNMO_850C_Na. The shape of the particles of samples LNMO_1350C_Na and LNMO_1350C are all rod-like (hexagonal) grains without obvious corner angles as shown in Figs. 2(c) and 2(d), respectively, and their average sizes are about 1 μm. These features are consistent with the XRD Rietveld refinement that the primary structure is $R\bar{3}$ phase in samples LNMO_1350C_Na and LNMO_1350C. In addition, the size distribution of the particles is more homogeneous using molten-salt fluxes.

Figures 3(a) and 3(b) show the magnetization M versus applied magnetic field H at different temperatures for samples LNMO_1350C and LNMO_750C_Na+K in the magnetic field range from −7 T to 7 T, consistent with a ferromagnetic feature at low temperatures. From the inset in Fig. 3(a), the values of the low-temperature saturation magnetization M_s at 2 K and 10 K are both $3.93\mu_B$/f.u., and thus, other samples are obtained for the values of M_s at 10 K. As shown in Fig. 3(b), the value of M_s at 10 K for sample LNMO_750C_Na+K is $3.05\mu_B$/f.u., which implies that this is a more disordered sample of the B-site cations. The predicted saturation magnetization value at low temperatures of LNMO is $M_s = 5\mu_B$/f.u., since Mn^{4+} and Ni^{2+} ions contribute three and two unpaired electrons,[25] respectively, the ferromagnetic order derives from the presence of 180° Ni^{2+}–O–Mn^{4+} superexchange bonding between an empty Mn^{4+} e_g orbital and a half-filled d orbital on a neighboring Ni^{2+} site from Kanamori–Goodenough rules.[26]

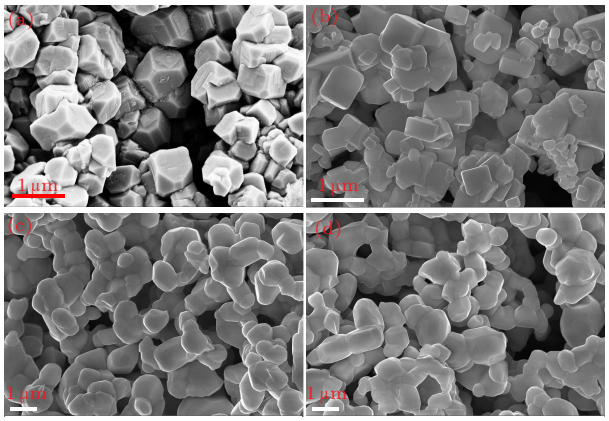

Fig. 2. SEM images of the samples LNMO_750C_Na+K (a), LNMO_850C_Na (b), LNMO_1350C_Na (c), and LNMO_1350C (d).

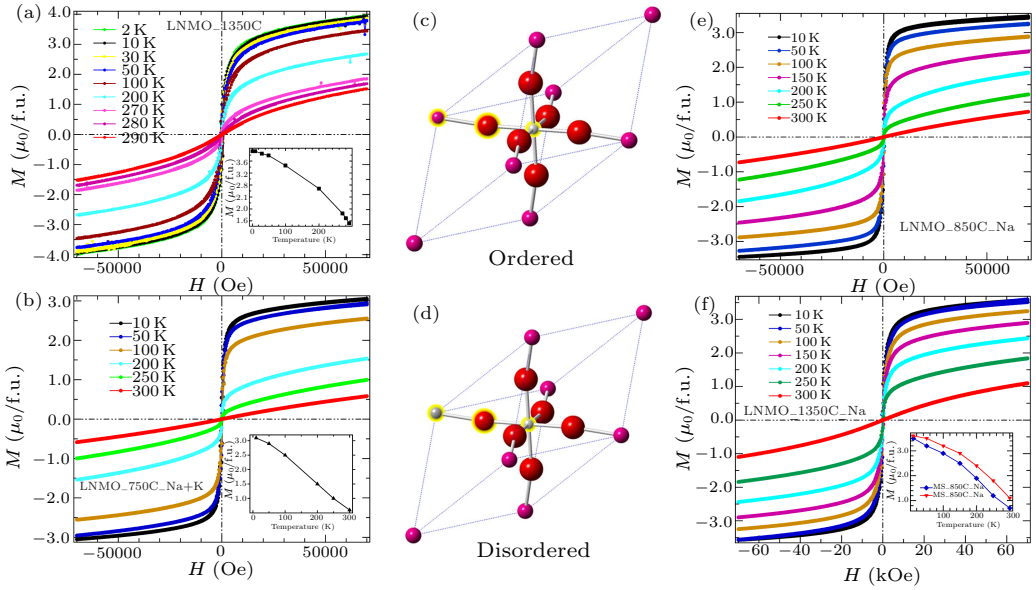

Fig. 3. SQUID data of samples LNMO_1350C (a) and LNMO_750C_Na+K (b), showing magnetic hysteresis loops measured at different temperatures. The insets at the bottom right corner show the values of the magnetism at 7 T. Schematic diagrams of the ordered (c) and partially disordered (d) LNMO sample in a rhombohedral structure without the La atoms. The highlighted atoms in the ordered and partially disordered structure represent the Ni^{2+}–O–Mn^{4+} ferromagnetic super-exchange, and Ni^{2+}–O–Ni^{2+} antiferromagnetic super-exchange interaction, respectively. Atom: Ni (gray), Mn (pink), and O (red). SQUID data of samples LNMO_850C_Na (e) and LNMO_1350C_Na (f), showing magnetic hysteresis loops measured at different temperatures. The inset in (f) shows the values of the magnetism at 7 T.

The influence of anti-site defects (ASD) on the low-temperature M_s can be exhibited by assuming the interchange of one Ni^{2+} with one Mn^{4+}, and *vice versa*. As shown in Fig. 3(c), for an ideally ordered LNMO sample with the rhombohedral structure, each Ni^{2+} ion is surrounded by six Mn^{4+} ions, and the highlighted atoms exhibit the Ni^{2+}–O–Mn^{4+} ferromagnetic super-exchange interaction; likewise, if the enter atom is Mn^{4+} ion, six Ni^{2+} ions will surround it. This feature is also equivalent in a monoclinic structure. However, as shown in Fig. 3(d), if a nearest Mn^{4+} ion is replaced by an Ni^{2+} ion, the central Ni^{2+} ion is surrounded by five Mn^{4+} ions and one Ni^{2+} ion, and *vice versa* for the central Mn^{4+}

ion. Therefore, in some local regions, the Ni^{2+}–O–Ni^{2+} and Mn^{4+}–O–Mn^{4+} antiferromagnetic superexchange interactions will dominate these defect sites due to the ASD. Thus, each ASD pair reduces the magnetic moment of the sample by $10\mu_B$. The relationship to the ASD and Q_{od} is $M_s = M_{sat} \times Q_{od} = M_{sat}(1 - 2[ASD])$,[3,4,16] where M_{sat} is the predicted saturation magnetization value at low temperatures of the ordered LNMO, the value of M_{sat} is $5\mu_B$/f.u., and [ASD] represents the ASD content. This prediction could be confirmed by the experimental results,[27] where the LNMO sample with antisite defect of ∼10% maintains 80% theoretical saturation magnetism at low temperatures (5 K). Thus, the ASD contents of samples LNMO_1350C and LNMO_750C_Na+K in this study could be ∼10.7% and ∼ 19.5%, respectively. Meanwhile, the ASD contents of samples LNMO_850C_Na ($M_s = 3.47\mu_B$/f.u.) and LNMO_1350C_Na ($M_s = 3.55\mu_B$/f.u.) are 15.3% and 14.5%, respectively, as shown in Figs. 3(e) and 3(f).

The values of M_s, ASD, Q_{od}, and the estimated average particle sizes Φ of these four samples are all summarized in Table 2. As listed in Table 2, the effects of the synthesized temperature and the flux on the Q_{od} or ASD is remarkable. Firstly, the ASD is decreased through increasing the synthesized temperature. Secondly, the ASD contents of sample LNMO_1350C_Na is obviously higher than that of sample LNMO_1350C, but only a slight lower than that of sample LNMO_850C_Na. This feature indicates that a higher annealing temperature cannot effectively eliminate the anti-site defects, if the contents of the ASD have been formed in LNMO sample at a lower temperature (such as 850℃). In comparison between LNMO_850C_Na and LNMO_1350C_Na, although their M_s values at 10 K is very close, the magnetism values at 7 T of LNMO_850C_Na are smaller than that of LNMO_1350C_Na when the measured temperatures from 50 K to 300 K [inset in Fig. 3(f)].

The thermal evolution of the magnetism susceptibility of these four samples are shown in Fig. 4. The ferromagnetic transition temperatures (T_c) of these samples are determined as the maximum value of dM/dT versus T curve,[28,29] and their values are listed in Table 2. As shown in Fig. 4(b), the $M(T)$ curve of sample LNMO_1350C is from a typical ferromagnetic LNMO sample with a saturation feature at a low temperature. However, samples LNMO_750C_Na+K, LNMO_850C_Na and LNMO_1350C_Na all have an anomaly feature at ∼160 K, which exhibit the enhancement of the $M(T)$ below ∼160 K. This feature could be induced by the antiferromagnetic Ni^{2+}–O–Ni^{2+} and Mn^{4+}–O–Mn^{4+} interactions because of a relatively higher concentration of ASD, which was also found in some LNMO samples by Dass *et al.*[24] This result is also explained by the inverse susceptibilities of the samples with the Curie Weiss law fitting in Fig. S1 and Table S1 in the Supplementary Material.

Table 2. Low-temperature saturation magnetism M_s, ASD, Curie temperature T_c and the estimated average particle sizes Φ of all samples.

Samples	M_s (μ_B/f.u.)	Q_{od}	ASD (%)	T_c (K)	Φ (nm)
LNMO_750C_Na+K	3.05	0.610	∼19.5	255	∼500–∼1000
LNMO_850C_Na	3.47	0.694	∼15.3	257	∼500
LNMO_1350C_Na	3.55	0.710	∼14.5	266	∼1000
LNMO_1350C	3.93	0.786	∼10.7	274	∼1000

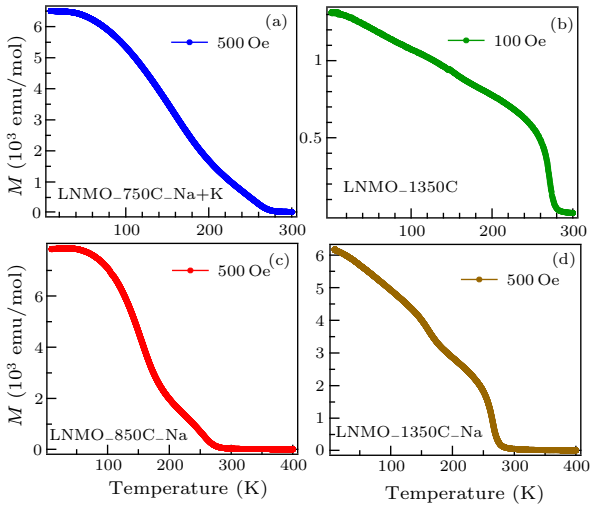

Fig. 4. Magnetization versus temperature of the sample (a) LNMO_750C_Na+K, (b) LNMO_1350C, (c) LNMO_850C_Na, and (d) LNMO_1350C_Na.

The B-site ordering of double perovskites results in a lowering of symmetry from holosymmetric $Pm\bar{3}m$ to $Fm\bar{3}m$,[21,30] in which Q_{od} has the symmetry of irreducible representation R_1^+. The lowest coupling terms between Q_{od} and magnetic ordering would be $\lambda Q_{od}^2 m_3^2$, and the main effect should be a renormalization of T_c in proportion to Q_{od}^2.[30,31] Thus, ignoring saturation terms in the Landau expansion, the new critical temperatures would be

$$T_c^* = T_c - \frac{2\lambda Q_{od}^2}{a_1}. \quad (1)$$

As shown in Fig. 5 including the data of our work and the literature,[1,3,16,17,24,27,32–39] one can find that the coupling coefficient λ is very weak since there is a confused dependence of the magnetic ordering temperature on the value of the Q_{od}^2. Our previous studies[4,16] and another report[24] have argued that this feature could be due to the oxygen stoichiometry, cation vacancy and other sample stoichiometry,

which is induced by the sample preparation process and conditions, like different annealing atmosphere and annealing temperature. Therefore, it is believable that the oxygen excess and individual particle size are primary factors to change the Curie temperatures of LNMO.[4,11,24] It should be noted that the individual LNMO particles could include one or more crystals, and normally a smaller particle has less percentage of the crystal boundaries. In addition, the samples summarized in Fig. 5 have shown that the thin films and single crystals, which have fewer crystal boundaries compared to the polycrystallines, have relatively higher values of $Q_{\rm od}$ and $T_{\rm c}$. This feature can be confirmed by the results of Nasir *et al.*,[40] showing an apparent decrease of the $Q_{\rm od}$ due to the increase of the particle sizes.

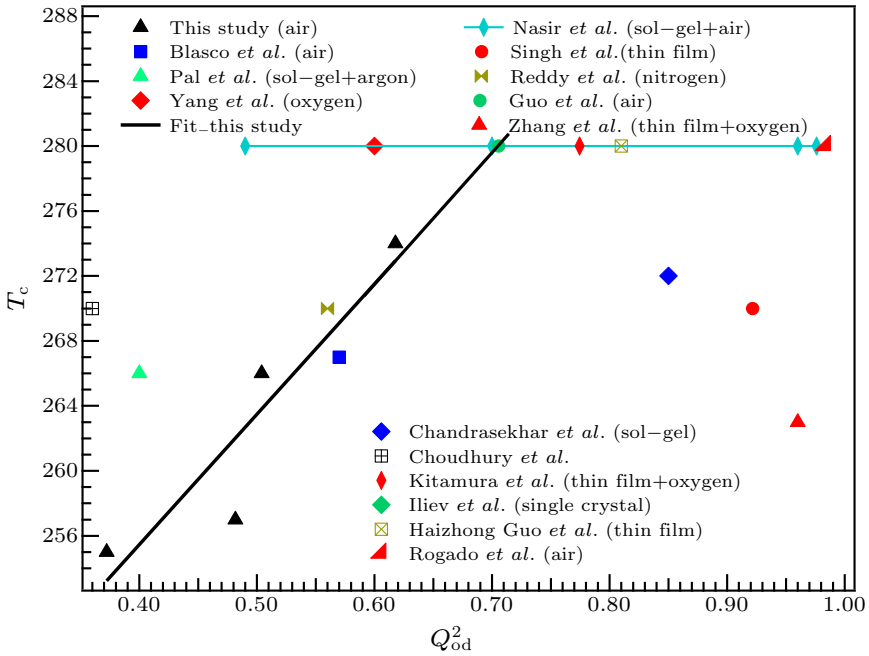

Fig. 5. Influences on the ordering degree of Ni/Mn ions, as expressed in terms of the order parameter $Q_{\rm od}$ on transition temperatures: compiled data from the literature[1,3,16,17,24,27,32–39] and the present study. Specific data sets are permissive for the expected relationships $T_{\rm c} \propto Q^2_{\rm od}$, however there is significant scatter which is probably due to other factors such as sample stoichiometries, sizes and prepared conditions.

The surprising result in Fig. 5 is that there appears to be an approximate linear relationship (black solid line) between $T_{\rm c}$ and $Q^2_{\rm od}$ for the samples prepared in this study and several other research results,[27,40,41] and these samples were all annealed in air. This result confirms that a similar annealing atmosphere will induce analogous oxygen stoichiometries of LNMO. In other words, it is possible that the $Q_{\rm od}$ will have a strong coupling effect with the new critical temperature $T^*_{\rm c}$ if the sample stoichiometries are close, like similar particle sizes, oxygen excess and cation vacancies. However, this prediction should be confirmed furthermore by a systematic investigation that can use the same experimental conditions in research groups.

In conclusion, multiferroic double perovskite LNMO has been successfully synthesized by the molten-salt-mediated method using eutectic NaCl/KCl mixtures at a low temperature (750℃). The extents of the Ni/Mn ordering can be modulated by controlling the synthesized temperature and selecting appropriate mediated salts. It is found that the coupling coefficient λ between the B-site cation ordering ($Q_{\rm od}$) and magnetic order parameter (m_3) is small, i.e., for weak coupling, based on the data taken from the literature and this study. However, if the LNMO sample stoichiometries are similar, we can find that $Q_{\rm od}$ and m_3 are some strong coupling effects due to the near-linear relationship between $T_{\rm c}$ and $Q^2_{\rm od}$ as the sample prepared in air. Although our results have partly confirmed the coupling effects between the Ni/Mn ordering and magnetic ordering, a systematic investigation under the same experimental conditions is necessary to further confirm the strength of the coupling coefficient λ.

References

[1] Rogado S, Jun Li, Sleight W and Subramanian A 2005 *Adv. Mater.* **17** 2225
[2] Wu S Q, Cheng S, Lu L, Liu M, Jin X W, Cheng S D and Mi S B 2018 *Sci. Rep.* **8** 2516
[3] Pal S, Sharada G, Goyal M *et al.* 2018 *Phys. Rev. B* **97** 165137
[4] Yang D, Lampronti G I, Haines H C R and Carpenter M A 2019 *Phys. Rev. B* **100** 014304
[5] Žutić I, Fabian J and Sarma S D 2004 *Rev. Mod. Phys.* **76** 323
[6] Fuertes A 2020 *APL Mater.* **8** 020903
[7] Yang X, Wang Y, Jiang J *et al.* 2020 *APL Mater.* **8** 021102
[8] Yang D and Huo D 2020 *J. Mater. Chem. C* **8** 6640

[9] Yang D, Yang T, Mukherjee P *et al.* 2019 *Phys. Rev. B* **99** 094314
[10] Tong Y, Wu J, Chen P *et al.* 2018 *J. Am. Chem. Soc.* **140** 11165
[11] Zhao S, Shi L, Zhou S *et al.* 2009 *J. Appl. Phys.* **106** 123901
[12] Iliev M N, Guo H and Gupta A 2007 *Appl. Phys. Lett.* **90** 151914
[13] Bull C L, Gleeson D and Knight K S 2003 *J. Phys.: Condens. Matter* **15** 4927
[14] Jin X W, Lu L, Mi S B, Liu M *et al.* 2016 *Appl. Phys. Lett.* **109** 031904
[15] Takahashi R, Ohkubo I, Yamauchi K, Kitamura M, Sakurai Y, Oshima M, Oguchi T, Cho Y and Lippmaa M 2015 *Phys. Rev. B* **91** 134107
[16] Yang D, Wang W, Yang T *et al.* 2018 *APL Mater.* **6** 066102
[17] Chandrasekhar K D, Das A K, Mitra C and Venimadhav A 2012 *J. Phys.: Condens. Matter* **24** 495901
[18] Fuoco L, Rodriguez D, Peppel T and Maggard A 2011 *Chem. Mater.* **23** 5409
[19] Arney D, Watkins T and Maggard A 2011 *J. Am. Ceram. Soc.* **94** 1483
[20] Porob G and Maggard A 2006 *J. Solid State Chem.* **179** 1727
[21] Howard J, Kennedy J and Woodward M 2003 *Acta Crystallogr. Sect. B: Struct. Sci.* **59** 463
[22] Carpenter M A 2015 *J. Phys.: Condens. Matter* **27** 263201
[23] Yang D, Chatterji T, Schiemer J A and Carpenter M A 2016 *Phys. Rev. B* **93** 144109
[24] Dass R I, Yan J Q and Goodenough J B 2003 *Phys. Rev. B* **68** 064415
[25] Das H, Waghmare U V, Saha-Dasgupta T and Sarma D D 2008 *Phys. Rev. Lett.* **100** 186402
[26] Goodenough B 1955 *Phys. Rev.* **100** 564
[27] Blasco J, García J, Sánchez M C, Campo J, Subías G and Pérez-Cacho J 2002 *Eur. Phys. J. B* **30** 469
[28] Palakkal J P, Sankar C R and Varma M R 2017 *J. Appl. Phys.* **122** 073907
[29] Yang D, Zhao P, Huang S, Yang T and Huo D 2019 *Results Phys.* **12** 344
[30] Yang D, Harrison J, Schiemer A, Lampronti I, Liu X, Zhang F, Ding H, Liu Y G and Carpenter A 2016 *Phys. Rev. B* **93** 024101
[31] Carpenter M A, Bryson J F J, Catalan G and Howard C J 2012 *J. Phys.: Condens. Matter* **24** 045901
[32] Sayed N, Achary S N, Jayakumar O D, Deshpande S K, Krishna P S R, Chatterjee S, Ayyub P and Tyagi A K 2011 *J. Mater. Res.* **26** 567
[33] Reddy M P, Shakoor R A and Mohamed A M A 2016 *Mater. Chem. Phys.* **177** 346
[34] Zhang Z, Jian H, Tang X, Yang J, Zhu X and Sun Y 2012 *Dalton Trans.* **41** 11836
[35] Choudhury D, Mandal P, Mathieu R, Hazarika A, Rajan S, Sundaresan A, Waghmare U V, Knut R, Karis O and Nordblad P 2012 *Phys. Rev. Lett.* **108** 127201
[36] Kitamura M, Ohkubo I, Kubota M, Matsumoto Y, Koinuma H and Oshima M 2009 *Appl. Phys. Lett.* **94** 132506
[37] Iliev M N, Gospodinov M M, Singh M P, Meen J, Truong K D, Fournier P and Jandl S 2009 *J. Appl. Phys.* **106** 023515
[38] Guo H, Gupta A, Varela M, Pennycook S and Zhang J 2009 *Phys. Rev. B* **79** 172402
[39] Singh M P, Grygiel C, Sheets W C, Boullay P, Hervieu M, Prellier W, Mercey B, Simon C and Raveau B 2007 *Appl. Phys. Lett.* **91** 012503
[40] Nasir M, Khan M, Kumar S *et al.* 2019 *J. Magn. Magn. Mater.* **483** 114
[41] Guo Y, Shi L, Zhou S, Zhao J and Liu W 2013 *Appl. Phys. Lett.* **102** 222401

Supplementary Material for

The effect of B-site ordering on the magnetic ordering in multifunctional La_2NiMnO_6 double perovskite

Dexin Yang[1**] (杨得鑫), Rui Jiang[1] (蒋蕊), Yaohua Zhang[1] (张耀华), Hui Zhang[1] (张辉), Senlin Lei[1] (雷森林), Tao Yang[1] (杨涛), Xiaoshi Hu[1] (胡小诗), Shuai Huang[1] (黄帅), Jingyuan Ge[2] (葛景园), Kunpeng Su[1] (苏昆朋), Haiou Wang[1] (王海鸥), Dexuan Huo[1**] (霍德璇).

[1]College of Materials & Environmental Engineering, Hangzhou Dianzi University, Hangzhou 310018, China;

[2]College of Chemistry and Materials Engineering, Wenzhou University, Wenzhou 325035, China.

[*]Supported by the National Natural Science Foundation of China (Grant No. 51702289, 21801054, 11604067), and Natural Science Foundation of Zhejiang Province (No. LQ20E020006).
[**]Corresponding author: (D. Y.) dy263@hdu.edu.cn; and (D. H.) dxhuo@hdu.edu.cn.

Table of Contents:

Detailed description of the Experimental methods.

Figure S1. The inverse susceptibilities of the sample (a) LNMO_750C_Na+K, (b) LNMO_1350C, (c) LNMO_850C_Na, and (d) LNMO_1350C_Na, with the fitting by Curie Weiss law.

Table SI. The fitting parameters by Curie-Weiss law of four LNMO samples, and the full width at half maxima (FWHM) of the intense XRD peak at around 32°.

II. EXPERIMENTAL METHODS

A. Sample preparation

Flux syntheses of La_2NiMnO_6 (LNMO) double perovskite were performed by first combining mixtures of analytical reagent grade La_2O_3 (Aladdin, 99.99%), NiO (Aladdin, 99.9%) and MnO_2 (Aladdin, 99.95%). The reactants were ground together and combined with a eutectic NaCl/KCl (Aladdin, 99.99%) mixture or only NaCl, and the flux: product molar ratio is 10:1. The powder mixtures were ground together in agate mortar and then heated to 750 ºC for sample with NaCl/KCl, or to 850 ºC and 1350 ºC for sample with NaCl in air. Correspondingly, they are labeled as LNMO_750C_Na+K, LNMO_850C_Na, and LNMO_1350C_Na, respectively. The reactions were all holding on 10 h and then slow cooled to room temperature of 1 ºC/min. The resulting powders were washed with hot distilled water to remove the NaCl/KCl or NaCl flux for sample LNMO_750C_Na+K and LNMO_850C_Na, respectively. For comparison, the traditional solid-state synthesis of LNMO were performed at 1350 ºC for 10 h in air by using a slightly modified procedure from the literature[1], and the resulting product powder was labeled as LNMO_1350C.

B. Characterization

X-ray diffraction (XRD) patterns of all samples were collected at room temperature on a Bruker-AXS D8 ADVANCE diffractometer operating in Bragg-Brentano geometry, equipped with a monochromator for primary Cu Kα radiation. To obtain the crystal information of these samples, Rietveld refinements were performed with the software TOPAS-Academic V6[2]. A shifted Chebyshev function with eight parameters and a pseudo-Voigt function (TCHZ type) were used to fit background and peak shape, respectively. The lattice parameters of the powder refinement are listed in Table I. To characterize the particle sizes and morphology of these samples, scanning electron microscopy (SEM, *FEI* and *ZEISS*) measurements were performed.

An MPMS-XL-7 quantum interference device (SQUID) was used to measure the field dependence of magnetization of sample LNMO_1350C at 2, 10, 30, 50, 100, 200, 270, 280 and 290 K in a magnetic field of up to 7 T. Temperature-dependent DC magnetic susceptibility of sample LNMO_1350C at 100 Oe from 2 K to 400 K were also measured at the same machine. The magnetic measurements of samples LNMO_750C_Na+K, LNMO_850C_Na, and LNMO_1350C_Na were measured on a Quantum Design Physical Properties Measurements System (PPMS), and their measured conditions are similar to sample LNMO_1350C.

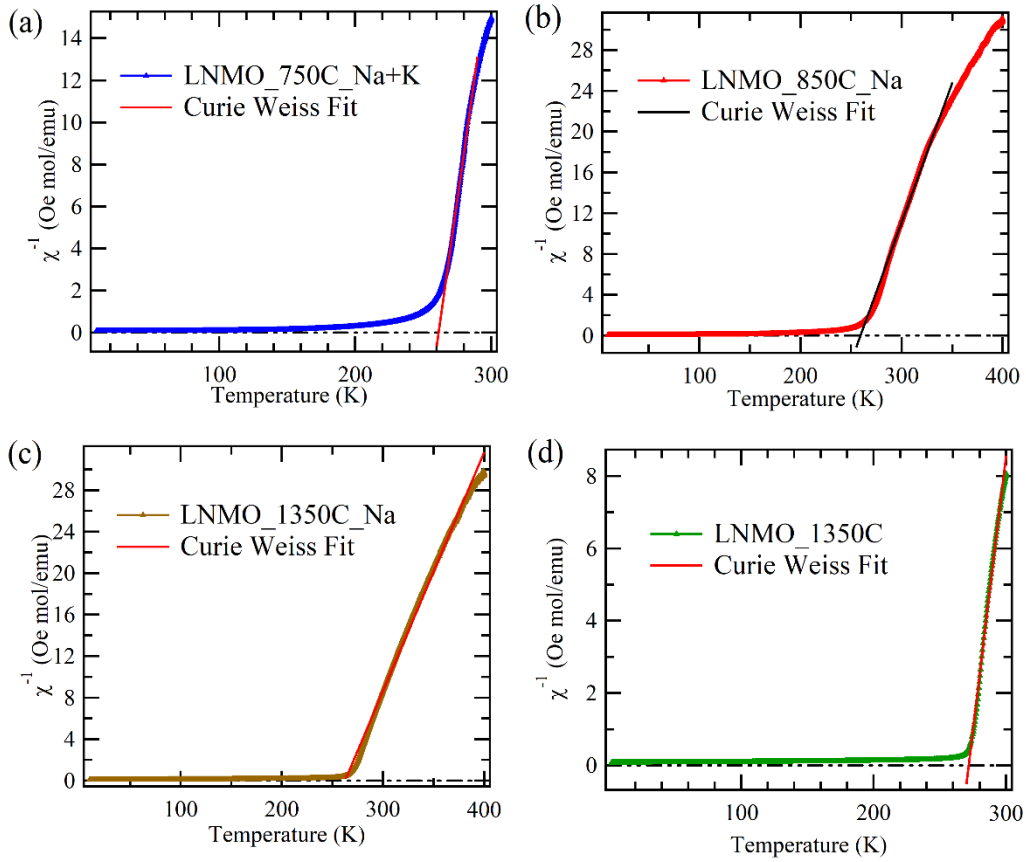

Figure S1. The inverse susceptibilities of the sample (a) LNMO_750C_Na+K, (b) LNMO_1350C, (c) LNMO_850C_Na, and (d) LNMO_1350C_Na, with the fitting by Curie Weiss law.

In the paramagnetic region, the magnetic susceptibility of these samples conforms to the Curie-Weiss law ($\chi = C/(T - \theta)$), where C is the Curie constant, and θ is the Curie-Weiss temperature, and thus the inverse susceptibility derived from the DC magnetic susceptibilities are shown in Figure S1. The inverse susceptibility, which is proportional to $(T - \theta)$, appears as a straight line (Figure S1), plotted as a function of temperature. A least squared error fitting approach is used to extract the Curie-Weiss temperature (θ), Curie constant (C), and the fitting parameters are listed in Table III. Then the effective paramagnetic moment μ_{eff} are calculated by $\mu_{eff} = 2.827\sqrt{C}$,[3] and the values are also shown in Table III. As expected for a ferromagnetic material, all samples possess the positive values of the Curie-Weiss temperature (θ), and the ASD has a negligible effect on Curie-Weiss temperature for these samples because of the very close values of θ. In other words, the super-exchange/ferromagnetic interaction between Ni^{2+} and Mn^{4+} ions, is not affected by the

presence of *B*-site disorder. However, there is an obvious reduction in the effective paramagnetic moment for sample LNMO_750C_Na+K, which has the most ASD among these samples. The lowering of the effective paramagnetic moment in the most disordered LNMO_750C_Na+K sample implies that higher contents of ASD will lead to the Ni^{2+}-O-Ni^{2+} and Mn^{4+}-O-Mn^{4+} antiferromagnetic interactions[3].

Table SI. The fitting parameters by Curie-Weiss law of four LNMO samples, and the full width at half maxima (FWHM) of the intense XRD peak at around 32°.

Samples	Curie-Weiss Temperature θ (K)	Curie constant C (emu K mol^{-1} Oe^{-1})	μ_{eff} (μ_B/f.u.)	FWHM at ~32°
LNMO_750C_Na+K	261.4	2.18	4.17	0.35
LNMO_850C_Na	259.2	3.66	5.41	0.49
LNMO_1350C_Na	262.4	4.35	5.90	0.29
LNMO_1350C	271.7	3.30	5.14	0.22

REFERENCES

1 Dexin Yang, Wei Wang, Tao Yang, Giulio I. Lampronti, Huijian Ye, Liankui Wu, Qiyao Yu, and Shaohua Lu, APL Materials **6** (6), 066102 (2018).

2 A. Cohelo, Coelho Software Brisbane, Australia (2007).

3 Somnath Pal, Govinda Sharada, Manik Goyal, Soham Mukherjee, Banabir Pal, Rana Saha, A. Sundaresan, Somnath Jana, Olof Karis, John W. Freeland, and D. D. Sarma, Physical Review B **97** (16), 165137 (2018).